Materials Science & Engineering A 570 (2013) 1–7

Contents lists available at SciVerse ScienceDirect

Materials Science & Engineering A

journal homepage: www.elsevier.com/locate/msea

Compression of crumpled aluminum thin foils and comparison with other cellular materials

O. Bouaziz [a,b,*], J.P. Masse [a], S. Allain [a], L. Orgéas [c], P. Latil [c]

[a] ArcelorMittal Research, Voie Romaine-BP30320, 57283 Maizières-lès-Metz Cedex, France
[b] Centre des Matériaux, Ecole des Mines de Paris, CNRS UMR 7633, B.P. 87, 91003 Evry Cedex, France
[c] CNRS/Université de Grenoble (Grenoble INP/UJF), Laboratoire Sols-Solides-Structures-Risques (3SR Lab), BP53, 38041 Grenoble Cedex 9, France

ARTICLE INFO

Article history:
Received 28 November 2012
Received in revised form
14 January 2013
Accepted 16 January 2013
Available online 24 January 2013

Keywords:
Crumpled materials
Self-locked architecture
Cellular materials
Foam
Elasticity
Plasticity

ABSTRACT

The elasto-plastic behavior of aluminum crumpled thin foils was characterized in close die and uniaxial compressions within a wide range of relative density with different initial sizes of sheet. The experiments highlight that crumpled materials can present a hybrid behavior between foams and entangled materials with an auxetic behavior up to a relative density of 15%.

1. Introduction

Interest of cellular materials for structural applications is mainly focusing on foams [1,2] forcompletereviewsand more recently on entangled materials [3–7] and truss structures [8–10]. On the other hand, in the last decade, randomly crumpled materials as polymerized membranes, biological cells and thin paper or metallic sheets, became a subject of great interest for physicists because of their fascinating topological properties and scaling laws [11–15].

Despite this literature, it is actually not possible to find experimental data for a complete comparison between crumpled materials and other cellular solutions for structural applications. This is the reason why this publication proposes a more complete characterization and analysis of the mechanical behavior of crumpled aluminum thin foils in a wide range of relative density. The results are discussed in regard to the knowledge concerning opened cell and closed cell foams and entangled metals as well.

2. Foams and entangled fibrous materials

In the case of cellular materials as foams and trusses, it has been theoretically and experimentally shown that the initial relative Young modulus E_0/E_s and yield strength σ_0/σ_s both are power-law like relations of the initial foam relative density ρ_0/ρ_s [1–2]

$$\frac{E_0}{E_s} \propto \left(\frac{\rho_0}{\rho_s}\right)^n \tag{1}$$

and

$$\frac{\sigma_0}{\sigma_s} \propto \left(\frac{\rho_0}{\rho_s}\right)^m \tag{2}$$

where the subscripts "0" and "*s*" refer to the properties of the foam and its bulk material, respectively, and where the typical values of the power-law exponent n and m are summarized in Table 1as a function of both the foam architecture and deformation meso-mechanisms, *i.e.* deformation mechanisms arising at the cell scale. When multiple deformation meso-mechanisms are involved, m and n take values in between those given by elementary mechanisms (see the third example given Table 1). Above the yield stress, elasto-plastic foams usually exhibit stress–strain curves with a horizontal plateau often ascribed to the progressive buckling of the cell walls.

For entangled fibrous materials, theoretical models and experimental evidences also yield to power-law like relations between the actual consolidation stress σ and their actual relative density ρ/ρ_s [16,17]. For such materials, it is often assumed that fibers are mainly bent during compression so that

$$\sigma \propto E_s\left(\left(\frac{\rho}{\rho_s}\right)^p - \left(\frac{\rho_c}{\rho_s}\right)^p\right) \tag{3}$$

ρ_c/ρ_s being a critical relative density below which the entangled fibrous media loose its mechanical integrity. For 3D

* Corresponding author at: ArcelorMittal Research, Voie Romaine-BP30320, 57283 Maizières-lès-Metz Cedex, France. Fax: +33 387 7047 12.
E-mail address: olivier.bouaziz@arcelormittal.com (O. Bouaziz).

0921-5093/$ - see front matter © 2013 Elsevier B.V. All rights reserved.
http://dx.doi.org/10.1016/j.msea.2013.01.031

Table 1
Classification of scaling laws for the compression of cellular materials as a function of their architecture and deformation meso-mechanisms.

Materials	Deformation meso-mechanisms	n	m
Open foam	Strut bending dominated	2	3/2
Truss	Strut stretching dominated	1	1
Closed foam (with thickening of edges)	Strut bending and plate stretching	$1<n<2$	$1<m<3/2$
Ideal closed foam (with no thickening of cell edges)	Plate bending dominated	3	2
Hexagonal honeycomb	Plate bending dominated	3	2

random fiber orientation, the power-law exponent p equals 3, whereas it is close to 5 and can rise up to 15–20 when the fiber orientation is planar random or nearly unidirectional[16–19]. Thus, upon loading, stress–strain curves exhibit a pronounced strain-hardening rather than a horizontal plateau.

3. Experimental procedure

3.1. Materials and sample preparation

In this study, standard aluminum foils (density $\rho_s=2.7$, thickness $t=20\,\mu m$) were used. They have an elasto-plastic behavior with a Young modulus $E_s=70$ GPa. Each foil was randomly crumpled and then inserted into a cylindrical die in order to obtain cylindrical samples for the compression tests (radius $R_0=16$ mm, height $h_0=30$ mm). To have a sufficiently wide experimental data base, miscellaneous crumpled samples with different initial relative densities ρ_0/ρ_s were produced by following such a processing route and by using different initial amounts of aluminum, *i.e.* different size L of square shaped aluminum foils, as summarized in Table 2.

To investigate the mesostructure of such materials, another smaller sample ($R_0=8$ mm, $h_0=20$ mm, $L=170.75$ mm, $\rho_0/\rho_s=14.5\%$) was produced by following the same processing route. This sample was then scanned inside a standard laboratory X-ray microtomograph (3SR Lab, RX Solutions apparatus, conical X-ray source, field of view of 1920×1536 pixels), allowing the sample mesostructure to be examined non-destructively. Therewith, the 3D and the 2D segmented micrographs represented in Fig. 1 have been extracted from the scanned sample (voxel size of $6.8\times6.8\times6.8\,\mu m^3$). Both of them illustrate the very particular mesostructure of these materials: the sole aluminum foil that was plastically and severely bent and distorted during the sample processing form a self-locked structure the topology of which (i) is roughly similar to some cellular materials and (ii) is somehow chaotic with many disordered ridges and curved thin walls. Besides, graphs plotted in Fig. 1(c and d) shows that within the all field of view, *i.e.* an 8 mm diameter and a 10 mm length cylinder centered inside the sample, the local relative density ρ_{0l}/ρ_s is approximately constant and rather close to ρ_0/ρ_s all along the height (Fig. 1c) and the radius (Fig. 1d) of the sample. Lastly, the Mean Intercept Length (*MIL*) method was used in order to estimate the Degree of Anisotropy *tDA* of the crumpled sample [20–22]. The value of *tDA* was equal to 1.4. It is close to 1, *i.e.* the value expected for isotropic mesostructure (*tDA* tends to infinity for a fully aligned structure): thus, it is fair to assume as a first approximation that produced crumpled samples exhibit isotropic mesostructures.

3.2. Close die compression experiments

As sketched in Fig. 2, the crumpled samples listed in Table 1 were subjected to close die compression experiments. For that purpose, each sample was put inside a cylindrical steel die ($R_0=16$ mm) mounted into a universal tensile testing machine (Zwick, load cell of 50 kN). Close die compaction experiments then consisted in subjecting the upper cylindrical punch of the apparatus (see Fig. 2) to a vertical downward motion at a low constant velocity ($0.17\ mm\ s^{-1}$). Hence, by recording during the tests both the compression force F and the actual sample height h (measured by a video extensometer with an accuracy of 1 μm), the average Cauchy stress σ, the compression Hencky strain ε and the actual sample relative density ρ/ρ_s could be respectively estimated as:

$$\sigma=\frac{F}{\pi R_0^2};\quad \varepsilon=\ln\left(\frac{h}{h_0}\right),\quad \frac{\rho}{\rho_s}=\frac{\rho_0}{\rho_s}\exp(-\varepsilon) \tag{4}$$

Furthermore, during the tests, the compression loading was reverted several times at various compression strains ε in order to further analyze the elasto-plasticity of the crumpled samples. In particular, these "load–unload" sequences were used to measure rigorously the close die longitudinal elastic modulus $E^*(\varepsilon)$ at the early beginning of the unloading stages

$$E^*(\varepsilon)=\frac{d\sigma}{d\varepsilon}(\varepsilon) \tag{5}$$

E^* was determined taking a correlation coefficient of 0.95 for criterion.

Table 2
Initial relative density and length of the initial aluminum sheet for each crumpled sample.

Sample	Initial relative density ρ_0/ρ_s	Initial length L (mm)
1	0.019	149.1
2	0.0237	166.7
3	0.0415	223.6
4	0.0536	250.9
5	0.078	295.0
6	0.0976	338.8
7	0.103	354.9

4. Results

4.1. Typical stress–strain curves

Fig. 3 shows a collection of stress–strain curves obtained during the close die compression of the samples listed in Table 2. As evident from this figure, the compression behavior is clearly elasto-plastic, whatever the considered initial relative density. Such an elasto-plasticity displays several noteworthy features:

- Crumpled samples exhibit an initial elastic behavior characterized by an initial modulus E_0^* up to an initial yield stress σ_0^*. The elastic to plastic transition is clearly marked, as with

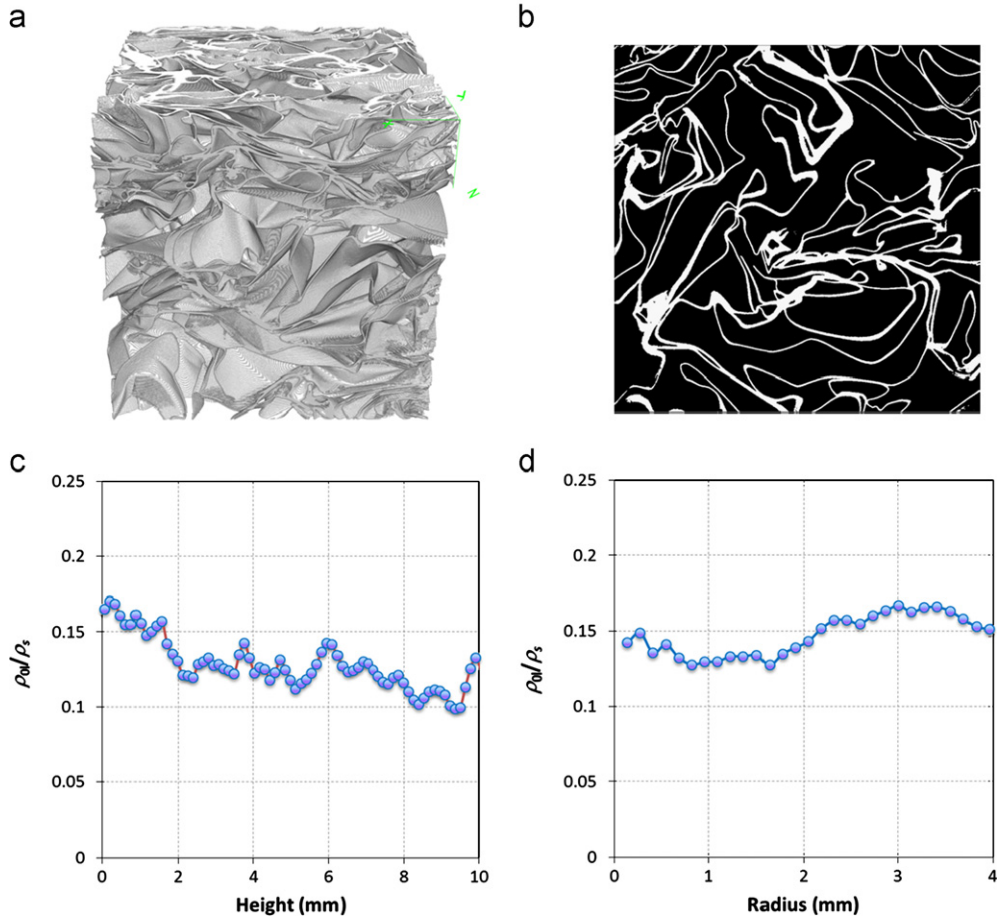

Fig. 1. (a) 3D (the Z axis is the compression axis, size$=6.8\times6.8\times6.8$ mm^3) and (b) 2D (perpendicular to the compression axis, size$=6.8\times6.8$ mm^2) segmented micrographs of a typical crumpled aluminum foil ($\rho_0/\rho_s=14.5\%$, obtained from X-Ray microtomography). Evolution of the local relative density ρ_{0l}/ρ_s along the height (c) and the radius (d) of the scanned sample.

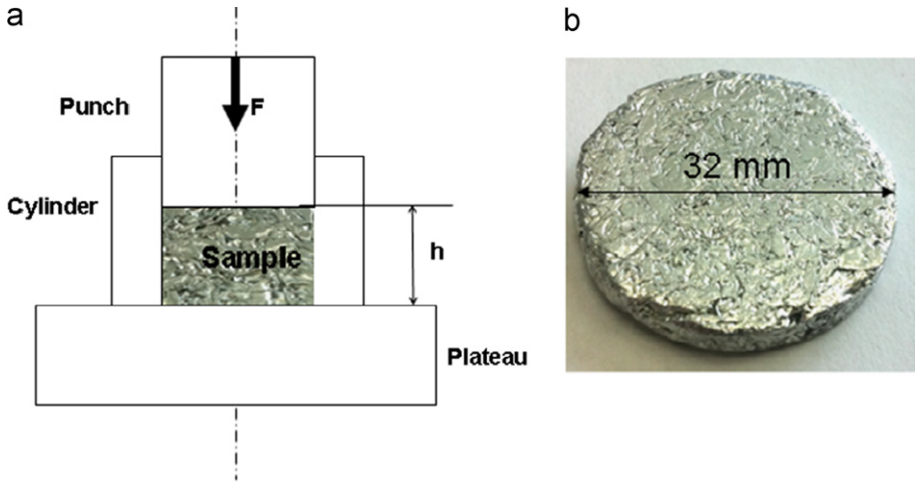

Fig. 2. (a) Schematic description of the close die compression device and (b) photograph of a deformed sample after a compression strain $\varepsilon=1.7$.

elasto-plastic foams (it is more difficult to identify it with entangled fibrous media).

- Above σ_0^*, the flow stress is an increasing function of the compression strain. This noticeable strain hardening is different from the horizontal plateau commonly observed during the consolidation of usual elasto-plastic foams [1–2]. It rather looks like the strain hardening observed in entangled fibrous materials.
- The elastic recovery after each unloading is non-linear but very limited, showing that the local deformation mechanisms occurring during the compression loading above the yield stress largely involve plastic deformation of aluminum foils.
- The unload–reload curves display very small hysteresis, with finishing points very close to their starting points, as if closed loops were shaped in the stress–strain diagram. Besides, once an unload–reload loop is completed, the loading curve recovers the

initial monotonic loading curve. Such an ideal elasto-plastic return point memory may be ascribed to a limited topological rearrangement of the aluminum foils during these sequences.

4.2. Elastic properties

The evolution of the relative close die longitudinal modulus E^*/E_s as a function of the actual relative density ρ/ρ_s is plotted in Fig. 4 (please note that the determination of E_0^*/E_s was achieved by the analysis reported in Appendix 1, *i.e.* by fitting E^*/E_s by affine function, E_0^*/E_s being taken as the value of these fits at $\rho/\rho_s=0$). As previously observed for other kind of cellular materials [1,2,5], it is clear from this figure that the relative elastic modulus E^*/E_s of the crumpled samples is not only a function of the actual relative density ρ/ρ_s but also a function of the initial relative density ρ_0/ρ_s (or, more generally, a function of the initial mesostructure of crumpled foils).

As illustrated in Fig. 5, the initial close die longitudinal modulus E_0^*/E_s can be expressed as a power-law of the initial relative density ρ_0/ρ_s:

$$\frac{E_o^*}{E_o^s}=0.127\left(\frac{\rho_o}{\rho_s}\right)^{1,82} \tag{8}$$

The transverse compression Poisson ratio v observed upon unloading the crumpled samples was also determined in order to see if its evolution with the relative density could exhibit wide range variations such as those observed for crumpled materials [15]. Therefore, in addition to close die compressions, uniaxial compressions were performed. New crumpled samples of 0.049 and 0.083 initial relative density were compressed in close die at different relative densities and then unloaded. After each unloading, the specimen was extracted from the close die and was loaded in uniaxial compression up to the beginning of plasticization followed by a final unloading for the measurement of the longitudinal Young modulus E. This operation was repeated for various relative densities. Therefore, by using standard isotropic elasticity relation

$$E^*=\frac{1-v}{(1+v)\ (1-2v)}E \tag{9}$$

It was then possible to estimate the transverse Poisson ratio v. Doing so, Fig. 6 proves that v experiences (i) significant variations with ρ/ρ_s and (ii) negative values below a relative density of 0.15,

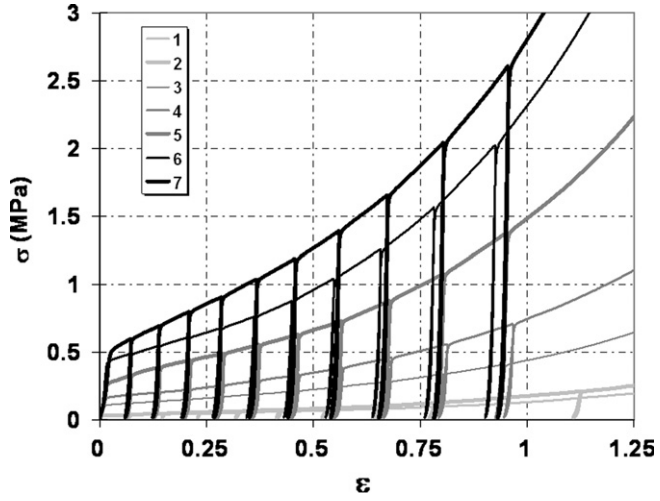

Fig. 3. Stress–strain curves obtained during the die compression (including load–unload sequences) of the crumpled aluminum samples listed in Table 2.

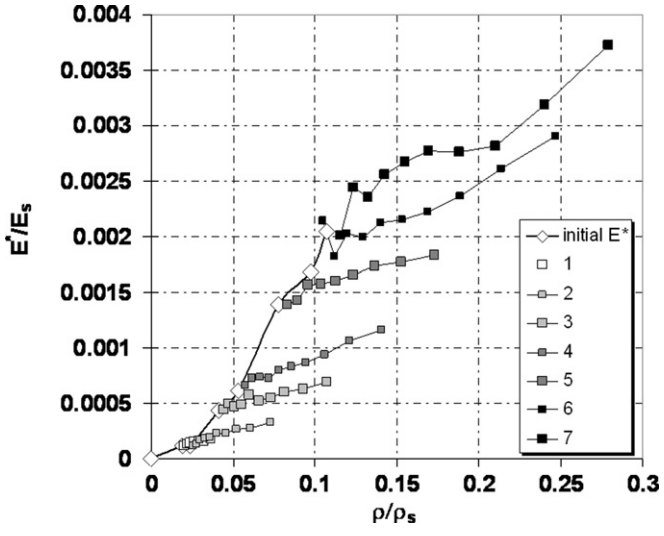

Fig. 4. Evolution of the relative close die longitudinal modulus with the relative density ρ/ρ_s of the crumpled aluminum samples listed in Table 2.

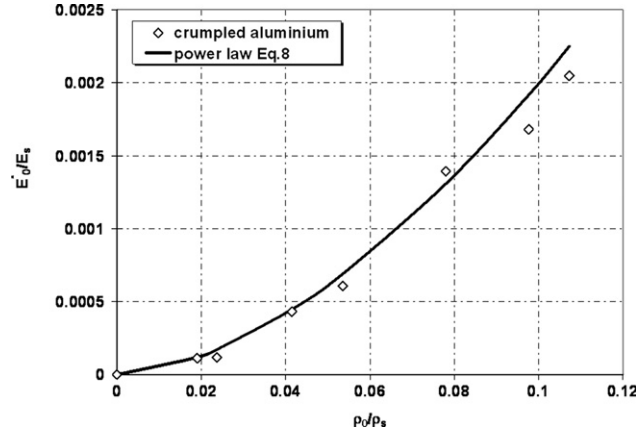

Fig. 5. Evolution of the initial longitudinal relative elastic close die modulus as a function of initial relative density of the tested samples.

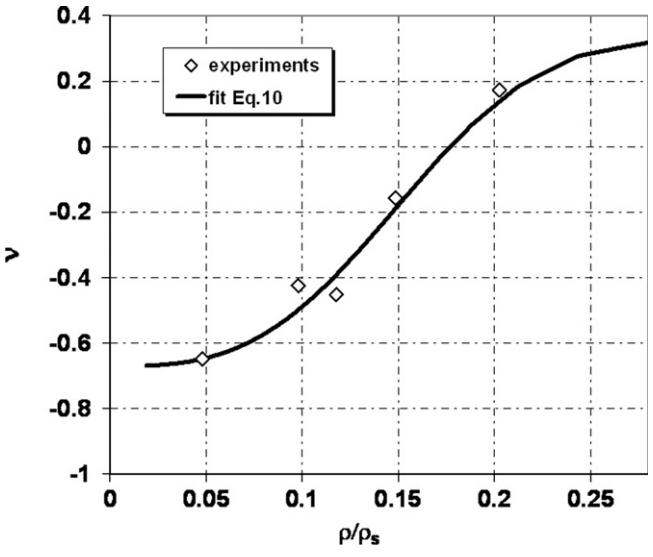

Fig. 6. Evolution of the Poisson ratio as a function of the relative density.

thus indicating an auxetic behavior within this density range. As also shown from this figure, a fairly good fit of v is:

$$v = v_s - \exp\left(-k\left(\frac{\rho}{\rho_s}\right)^q\right) \tag{10}$$

with $v_s = 0.33$, $k = 200$ and $q = 3$.

This analysis neglects the effect of friction. This assumption seems reasonable because the very low hysteresis observed for the unloading–reloading tests in close die illustrated in Fig. 3 confirms that the effect of friction is very low.

By using this fit and by returning to Eq. (9), it was then possible to estimate the initial relative Young modulus E_0/E_s of samples listed in Table 2, as illustrated in Fig. 7. Such an evolution is well-fitted by the following power-law:

$$\frac{E_0}{E_s} = 0.4\left(\frac{\rho_0}{\rho_s}\right)^{2.4} \tag{11}$$

In the case of foams, the power-law exponent $n = 2.4$ is consistent with deformation meso-mechanisms ruled both by plate and strut bending (see Table 1). In the case of crumpled samples, this would indicate that both the bending of the ridges and the thin walls could be involved.

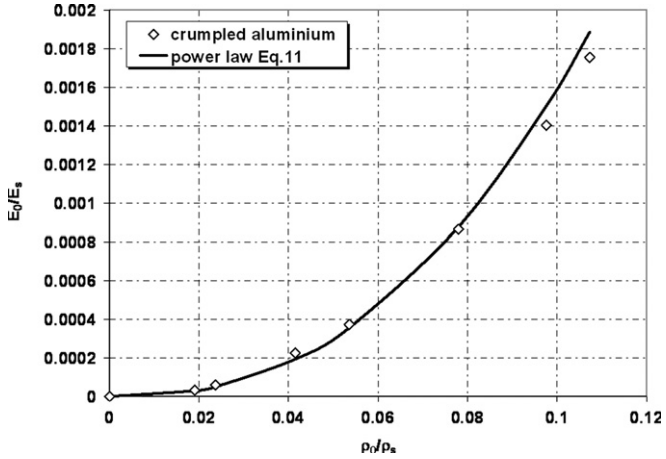

Fig.7. Evolution of the relative initial Young modulus as a function of the initial relative density.

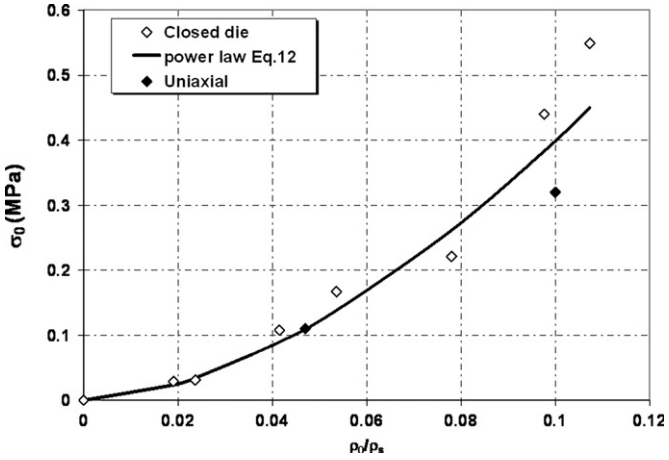

Fig. 8. Yield stresses σ_0^* and σ_0 as functions of the initial relative density for crumpled aluminum.

4.3. Yield stress

From the experiments shown previously, yield stresses σ_0^* and σ_0, respectively measured during close die and uniaxial compression were also extracted. Corresponding results have been gathered in Fig. 8. They first show that close die and uniaxial yield stresses follow the same trend and exhibit a small difference (this has to be confirmed by additional experimental data). Fig. 8 also shows that the close die yield stress σ_0^* is a power-law of the initial relative density

$$\sigma_0^* = 20\left(\frac{\rho_0}{\rho_s}\right)^{1.7} \tag{12}$$

which would indicate plastic deformation meso-mechanisms involving the bending of both the crumpled samples ridges and thin walls (see Table 1).

4.4. Flow stress and densification

For each sample, a noticeable increase of stress levels is observed after reaching the yield stress σ_0^*, due to the packing of the crumpled specimen. This is not what is observed in the case of foams for which a horizontal plateau stress is often observed before the last stiff densification stages. In the case of crumpled samples, it seems that packing mechanisms rather resemble to those observed with entangled materials, for which packing progressively occurs by a regular increase of the fiber coordination number (or the number of fiber–fiber contacts per fiber). As shown in Fig. 9, the densification of all the samples can be described as for $\sigma \geq \sigma_0^*$

$$\sigma \propto \left(\frac{\rho}{\rho_s}\right)^p \tag{13}$$

where $1.5 \leq p \leq 1.7$. This flow stress evolution as a function of the relative density of crumpled samples is qualitatively consistent with entangled materials (power-laws with $3 \leq p \leq 5$) but with a power-law exponent obviously lower.

It is interesting to note that the power-law exponents obtained for the yield (Eq. (12)) and flow (Eq. (13)) stresses are nearly identical. This first suggests that the same deformation meso-mechanisms were involved during both the fabrication and the compression of the samples. Combined with the return point memory effect emphasized

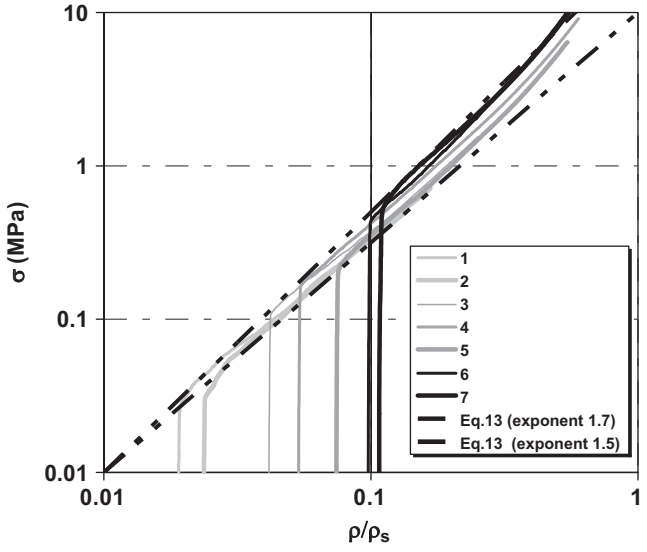

Fig. 9. Close die flow stresses as functions of the initial relative density for crumpled aluminum.

in Fig. 3, this also means that it is possible to extrapolate the yield stress estimation Eq. (12) for relative densities higher than 0.1, *i.e.* up to relative density close to 0.4.

5. Comparison with foams

From the data gathered in the previous sections together with their associated fits, the specific elastic and plastic properties of crumpled aluminum thin foils are now compared with those of standard aluminum foams (data collected from [1]). For that purpose, the specific Young modulus and yield stress of crumpled aluminum foils and aluminum foams were reported in the graphs of Figs. 10 and 11, respectively (including extrapolation for yield stress for relative density up to 0.4). Bearing in mind that crumpled foils are only self-locked architectures, *i.e.* porous mesostructures without any strong chemical bonds at the mesoscale, their specific rigidity and strength are surprisingly rather well positioned in these graphs. In particular, it appears that such cheap crumpled solutions may be competitive for specific bending stiffness $E^{1/3}/\rho$. Likewise, the specific bending strength $\sigma_0^{1/2}/\rho$ of crumpled aluminum foils seems also to be competitive.

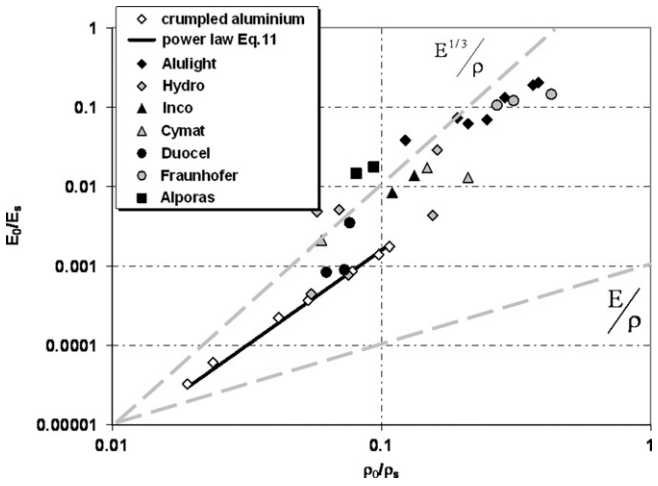

Fig. 10. Comparison of elastic modulus as a function of relative density for crumpled aluminum thin foils and aluminum foams, trend of performance index for bending and tension are added.

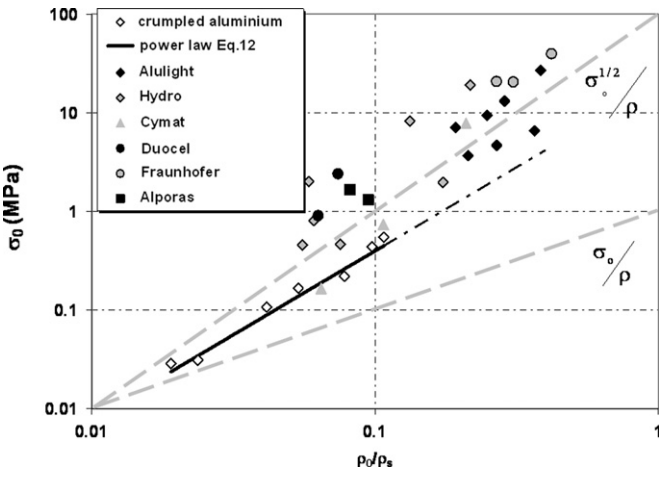

Fig. 11. Comparison of yield stress as a function of relative density for crumpled aluminum thin foils and aluminum foams, trend of performance index for bending and tension are added.

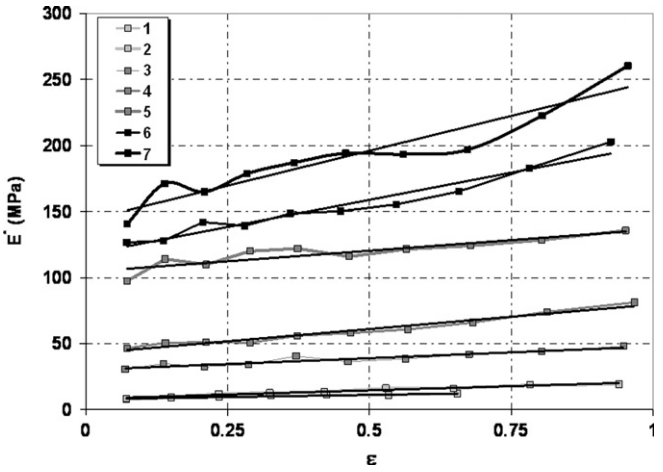

Fig. A1. Evolution of the close die longitudinal modulus with the Hencky strain for the determination of the initial close die longitudinal modulus .

6. Conclusion

In conclusion, our experiments seem to highlight that crumpled materials can present a hybrid mechanical behavior, between foams and entangled fibrous materials. They exhibit a clear plasticity and a low hysteresis as foams but no plateau beyond the yield stress. Instead, a strain hardening occurs directly after reaching the yield stress.

As this aspect is scientifically intriguing and as crumpled materials can have potential use for structural applications due the good combination between properties, density and an easy way to process, it is planned in the future to improve understanding in this field, especially using X-ray tomography investigations. As illustrated in Fig. 1, preliminary trials performed by authors indicate that the technique is well adapted to characterize the mesostructure of crumpled materials. The final issue is to better describe the crumpling phenomenon and to establish the link between the macroscale mechanical behavior and the developed complicated internal mesostrcutre. It is also required to investigate different initial configuration as foils with different thickness and made of different materials.

Acknowledgments

The authors thank Benjamin Bouaziz for stimulating discussions.

Appendix A1

The initial close die longitudinal elastic modulus was determined by the following method. As shown in figure X the close die longitudinal elastic modulus can be fitted by a linear equation as a function of the strain express as

$$E^* \propto E_0^* + b\varepsilon \tag{A1}$$

where b is the slope and E_0^* the initial close die longitudinal elastic modulus.
See Fig. A1

References

[1] M.F. Ashby, A.G. Evans, N.A. Fleck, L.J. Gibson, J.W. Hutchinson, H.N.G. Wadley, Metal Foams: A Design Guide, Butterworth–Heinemann, Boston (MA), 2000.
[2] L.J. Gibson, M.F. Ashby, Cellular Solids: Structure and Properties, second ed., Cambridge University Press, Cambridge, 1999.
[3] D. Poquillon, B. Viguier, E. Andrieu, J. Mater. Sci. 40 (2005) 5963.

[4] M. Baudequin, G. Ryschenkow, S. Roux, Eur. Phys. J. B 12 (1999) 157.
[5] J.P. Masse, L. Salvo, D. Rodney, Y. Bréchet, O. Bouaziz, Scr. Mater. 54 (2006) 1379.
[6] C. Barbier, R. Dendievel, D. Rodney, Phys. Rev. E 80 (2009) 16115.
[7] O. Bouaziz, J.P. Masse, Y. Bréchet, Scr. Mater. 64 (2011) 107.
[8] G.W. Kooistra, V.S. Deshpande, H.N.G. Wadley, Acta Mater. 52 (2004) 4229.
[9] E. Bele, B.A. Bouwhuis, G.D. Hibbard, Mater. Sci. Eng. A 489 (2008) 29.
[10] B.A. Bouwhuis, B. Chehab, O. Bouaziz, D. Embury, H. Zurob, G.D. Hibbard, Scr. Mater. 63 (2010) 609.
[11] B.A. DiDonna, T.A. Witten, Phys. Rev. Lett. 87 (2001) 206105.
[12] K. Matan, R.B. Williams, T.A. Witten, S.R. Nagel, Phys. Rev. Lett. 88 (2002) 076101.
[13] A.S. Balankin, O.S. Huerta, R.C. Montes de Oca, D.D. Ochoa, J.M. Trinidad, M.A. Mendoza, Phys. Rev. E 74 (2006) 061602.
[14] G.A. Vliegenthart, G. Gompper, Nat. Mater. 5 (2006) 216.
[15] A.S. Balankin, D. Samayoya Ochoa, E. Pineda-Leon, R.C. Montes de Oca, A. Horta Rangel, M.A. Matrinez-Cruz, Phys. Rev. B 77 (2008) 125421.
[16] C.M. Van Wyk, J. Text. Inst. 37 (1946) 285.
[17] S. Toll, Polym. Eng. Sci. 38 (1998) 1337.
[18] J.P. Masse, D. Poquillon, Scr. Mater. 64 (2012) 107.
[19] P. Latil, L. Orgéas, C. Geindreau, P.J.J. Dumont, S. Rolland du Roscoat, Compos. Sci. Technol. 71 (2011) 480–488.
[20] A. Odgaard, Bone 20 (20) (1997) 315–328.
[21] T.P. Harrigan, R.W. Mann, J. Mater. Sci. 19 (1984) 761–767.
[22] M. Doube, M.M. Kłosowski, I. Arganda-Carreras, F. Cordeliéres, R.P. Dougherty, J. Jackson, B. Schmid, J.R. Hutchinson, S.J. Shefelbine, Bone 47 (2010) 1076–1079.